UJEAS

UNIZIK JOURNAL OF ENGINEERING AND APPLIED SCIENCES

UNIZIK Journal of Engineering and Applied Sciences 6(4), December (2026), 3890-3903
Journal homepage: https://journals.unizik.edu.ng/index.php/ujeas
PRINT ISSN: 2992-4383 || ONLINE ISSN: 2992-4391

Effects of Welding Current on the Mechanical and Microstructural Properties of Gas Metal Arc Welded 304 Austenitic Stainless-Steel Joints

Echoida, Hussein Mohammed[1]* Akindapo, Jacob Olaitan[1] and Orueri, Daniel Ufuoma[1]*

[1]*Department of Mechanical Engineering, Faculty of Engineering, Nigerian Defence Academy, Kaduna, Nigeria*

*Corresponding Author's E-mail: echoida.hussein@nda.edu.ng; danielorueri@nda.edu.ng

Abstract
This study evaluates the effect of welding current on the mechanical properties, microstructure, defect formation, and chemical composition of 304 austenitic stainless-steel joints produced by gas metal arc welding (GMAW). Plates were welded at 90 A, 110 A, and 130 A, with arc voltage, welding speed, and electrode type held constant to isolate the effect of current on heat input. Welded specimens underwent tensile, impact, and hardness testing, metallography, non-destructive testing (NDT), and optical emission spectrometry (OES) analysis. The 110 A specimen performed best overall, with the highest ultimate tensile strength (550 MPa), yield strength (420 MPa), and impact energy absorption (72 J), fracturing in the base metal rather than the weld. Hardness rose in the weld metal with increasing heat input while the heat-affected zone (HAZ) softened correspondingly. Excessive current caused HAZ grain coarsening and, at higher heat input, carbide precipitation and sensitization; insufficient current produced incomplete fusion and porosity. NDT confirmed 110 A welds were essentially defect-free, while low- and high-heat-input welds showed porosity and surface cracking, respectively. OES confirmed parent and weld metal conformed to the standard composition of Grade 304 stainless steel. Welding current is thus established as a controlling variable in weld integrity, with 110 A identified as the optimum condition for mitigating weld cracking in industrial fabrication.
Keywords: *Austenitic stainless steel; Gas metal arc welding; Welding current; Heat input; Microstructure*

1. Introduction

Welding is the process of joining two or more pieces of metal by heating them to a temperature sufficient to cause softening or melting, with or without the application of pressure and with or without a filler metal (Kou, 2020). It remains one of the most widely used fabrication techniques in modern engineering, applied in pressure vessels, structural steelwork, pipelines, and food-processing equipment. Among the arc welding processes in industrial use, gas metal arc welding (GMAW) is particularly attractive for stainless steel fabrication because it concentrates heat at a focal point, producing deep penetration, a narrow bead width, and a comparatively small heat-affected zone (HAZ), while its continuous wire feed permits high deposition rates and reduced post-weld cleaning (Lippold and Kotecki, 2019).

Type 304 austenitic stainless steel is the most widely used stainless steel grade, combining good corrosion resistance, weldability, toughness, and formability by virtue of its 18-20% chromium and 8-10.5% nickel content. Despite its favourable weldability relative to other stainless-steel classes, 304 stainless steel remains sensitive to the thermal cycles imposed during fusion welding. Chromium carbides can precipitate at grain boundaries in the temperature range of approximately 450-850 °C, a phenomenon known as sensitization, which depletes chromium from the surrounding matrix and increases susceptibility to intergranular corrosion and surface cracking (Ramkumar and Mishra, 2018; Suresh *et al.* 2020). Uncontrolled or excessive heat input can additionally promote grain coarsening in the weld metal and HAZ, reducing strength and toughness, while insufficient heat input can cause incomplete fusion, lack of penetration, and porosity (Kumar *et al.* 2019).

A substantial body of recent work has examined how welding parameters govern the mechanical and metallurgical outcome of fusion-welded joints. Kumar *et al.* (2020) showed that tool rotational speed strongly affects the mechanical properties of friction-stir-welded aluminium alloy 5083, with an optimum speed of 600 rev/min producing the best combination of strength and ductility, a parameter-optimization logic that parallels the present investigation of welding current in GMAW. Amit *et al.* (2016) applied Taguchi-based grey relational analysis to GMAW of AISI 1020 carbon steel and found that welding speed, voltage, and current contributed 90.08%, 4.55%, and 0.66%, respectively, to weld bead geometry, underscoring that even a comparatively small percentage contribution from current can still be practically decisive for penetration and fusion quality.

Specifically for austenitic stainless steels, Zhang *et al.* (2019) demonstrated that optimized GMAW parameters yield sound weld joints with improved mechanical properties and reduced susceptibility to surface cracking, while Chen *et al.* (2020) showed that microstructural evolution under varying GMAW parameters directly controls the mechanical behaviour of 304 stainless steel weldments. Ghosh *et al.* (2021) found that welding heat input has a marked effect on the toughness of austenitic stainless-steel joints, and Zhao *et al.* (2019) reported that hardness distribution and phase composition in 304 stainless steel weldments vary systematically with welding conditions. Mohammed *et al.* (2021) specifically examined surface cracking in stainless steel welds, attributing it to uncontrolled thermal cycling, and proposed heat-input control as a primary mitigation strategy, a finding of direct relevance to the industrial cracking problem motivating the present work. Singh *et al.* (2019) further showed that arc voltage governs weld-bead geometry and defect formation in GMAW of stainless steel, while Shanmugam *et al.* (2019) linked optimum welding current to improved tensile properties through a refined microstructure and reduced weld discontinuities.

The novelty of the present study lies in its integrated, multi-technique evaluation of a single controlled variable, welding current, across four complementary characterization domains, namely tensile behaviour, impact toughness, hardness distribution, and microstructure, corroborated by non-destructive testing and optical emission spectrometry (OES) chemical composition analysis. Rather than treating these as independent parametric outcomes, as is common in the literature reviewed above, the study cross-validates the mechanical, metallurgical, and quality-assurance evidence against one another within a single controlled experiment, and frames the investigation around an industrially motivated case, the recurring surface cracking of stainless-steel joints observed at a food-processing facility, rather than a purely academic parametric dataset. This combined approach strengthens the basis for recommending an optimum GMAW current for 304 stainless steel fabrication and links the recommendation directly to an observed field failure mode.

Although the reviewed studies individually establish that welding current and heat input govern penetration, grain size, hardness, and defect formation in stainless steel and related alloys, comparatively few integrate mechanical testing, microstructural characterization, non-destructive evaluation, and chemical composition analysis within a single controlled experiment isolating welding current specifically for GMAW-joined 304 stainless steel under industrially representative conditions. This is the specific gap addressed by the present study. Accordingly, the objectives of the study were to: (i) determine the chemical composition of the parent metal and weld metal; (ii) evaluate the effect of welding current on the tensile, impact, and hardness properties of the weldment; (iii) characterize the microstructure of the weld metal, HAZ, and base metal for each welding condition; (iv) inspect the welded joints using non-destructive testing methods; and (v) validate the findings against previously published results, thereby providing an evidence-based, practically applicable recommendation for optimum GMAW current in 304 stainless steel fabrication.

2.0 Materials and Methods

2.1 Materials

The materials used in this study comprised 304 austenitic stainless-steel plate as the base metal, AISI 304 (E308L) stainless steel filler wire of 3.2 mm diameter, argon shielding gas of 99.9% purity, dilute sulphuric acid (0.2 M) as the metallographic etchant, 95% ethanol, distilled water, cotton wool, polishing cloth and polishing powder, and silicon carbide grinding papers of 120 and 600 grit.

2.2 Equipment

The equipment used for specimen fabrication and testing is summarized in Table 1. Experimental work was carried out at the Defence Industries Corporation of Nigeria (DICON), Kaduna, with hardness testing conducted using a Micro Vickers hardness tester.

Table 1: Equipment used in the experimental work

S/N	Equipment	Specification
1	Oxy-acetylene welding equipment	Standard industrial type, 3100 °C
2	GMAW welding machine	250 A, DC inverter
3	Grinding machine	240/250 V AC
4	Micro Vickers hardness tester	Model MVI-PC
5	Optical emission spectrometer (OES)	Model PDA 7000
6	Avery Izod impact testing machine	Model 51425/G
7	Dennison tensile testing machine	500 kN, Model T42B2
8	Metallurgical microscope	Trinocular, 40x-1000x, Model NJF120
9	Welding accessories	Oxy-acetylene set, goggles, torch
10	Chipping hammer / bench vice	Standard workshop type

2.3 Specimen Preparation and Welding Procedure

304 austenitic stainless steel plates were cut to 55 x 150 mm using a cutting machine and vice, and edge-prepared as a single-V butt joint with a broad root face in accordance with EN ISO 9692-1:2013 (Fig. 1), with a groove angle of 60 degrees machined on a milling machine and a root opening of 1.5 mm. Prior to welding, plate surfaces were degreased and cleaned with acetone to remove oil, grease, mill scale, and other surface contaminants that could otherwise promote porosity or lack of fusion.

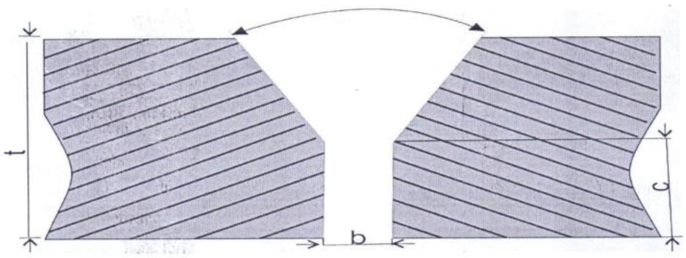

Figure 1: Cross-section of the single-V butt joint edge preparation (t = base-metal thickness; b = root opening; c = root face thickness; a = groove angle).

Welding was carried out by GMAW using ER308L filler wire under an argon shielding gas envelope, with the plates positioned approximately 2 mm apart and welded using the rightward (backward) technique. A schematic of the GMAW process is shown on Fig. 2. Three welding currents were investigated: 90 A (low), 110 A (medium), and 130 A (high), while arc voltage (24 V), welding speed (3 mm/s), electrode type (E308L), and electrode diameter (3.2 mm) were held constant, so that any change in weld quality could be attributed to welding current and its associated heat input. A fourth condition, representing an excess heat input beyond the high-current setting, was also examined to establish the upper boundary of acceptable performance. The multi-pass welding procedure (root, hot/fill, and cap passes) is summarized in Table 2. Arc voltage and travel speed were held constant at 24 V and 180 mm/min (3 mm/s), respectively, across all three passes and across all three welding-current conditions (90 A, 110 A, 130 A), consistent with the parameters reported in Table 3; only the welding current shown in Table 2 (110 A) is illustrative of the pass sequence, with the current for each pass adjusted proportionally for the 90 A and 130 A specimens while voltage and travel speed remained fixed.

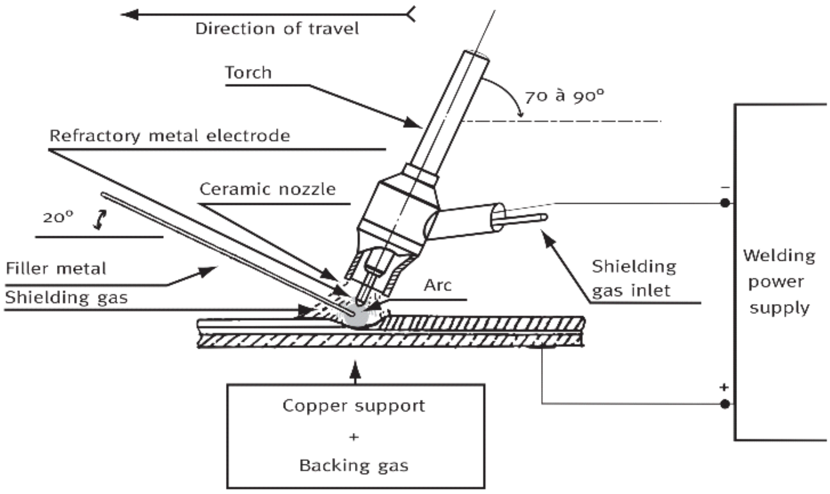

Figure 2. Schematic representation of the gas metal arc welding (GMAW) process.

Table 2: Multi-pass GMAW welding procedure

Welding Pass	Current (A)	Arc Voltage (V)	Travel Speed (mm/min)
1 (root pass)	110	24	180
2 (hot and fill pass)	110	24	180
3 (cap pass)	110	24	180

The overall welding parameters used to isolate the effect of current are summarised in Table 3. Heat input, which combines the effect of current, voltage, and welding speed, was computed using Eq. (1):

$$H = \frac{V \times I \times 60}{S \times 1000} \quad (1)$$

where H is the heat input (kJ/mm), V is the arc voltage (V), I is the welding current (A), and S is the welding speed (mm/min). Because V and S were held constant, variation in H across specimens is attributable to welding current alone.

Table 3: Welding parameters used in experimental work

Parameter	Value
Welding current	90 A, 110 A, 130 A
Arc voltage	24 V
Welding speed	3 mm/s
Electrode type	E308L
Electrode diameter	3.2 mm
Shielding gas	Argon, 99.9% purity

2.4 Chemical Composition Analysis

The chemical composition of the parent metal and weld metal was determined using an Optical Emission Spectrometer (OES, Model PDA 7000). Prepared samples were subjected to spark excitation, which vaporizes a small volume of the metal surface and excites its constituent atoms to emit light at characteristic wavelengths; this emitted light was resolved by an optical grating into its constituent wavelengths and converted into measurable intensities by a detector, from which the elemental composition was computed against factory calibration curves. Results were compared to the standard composition range for Grade 304 stainless steel.

2.5 Mechanical Testing

2.5.1 Tensile Test

Tensile testing followed EN ISO 4136:2012. Specimens were polished with 8000-grit SiC paper to remove surface flaws prior to testing, mounted in a Universal Testing Machine of 100 kN capacity (cross-checked against the 500 kN Dennison tensile machine), and loaded axially at a strain rate of 0.5 kN to fracture. Three specimens were tested per condition and the average recorded. Engineering stress and strain were computed using Eqs. (2) and (3):

$$\sigma = \frac{F}{A_0} \quad (2)$$

where σ is engineering stress (MPa), F is applied force (N), and A_0 is the original cross-sectional area (24 mm^2 for all specimens, corresponding to a sub-size proportional flat specimen with gauge width 4.8 mm, thickness 5.0 mm (equal to the plate thickness), and parallel gauge length 25 mm, in accordance with EN ISO 4136:2012).

$$\varepsilon = \frac{\Delta L}{L_0} \quad (3)$$

where ε is engineering strain, ΔL is elongation, and L_o is the original gauge length. Ultimate tensile strength, 0.2% proof (yield) stress, elongation at failure, and fracture location were recorded for each specimen.

2.5.2 Impact Test

Charpy V-notch impact testing was performed in accordance with EN ISO 9016:2012 (specimen location and notch orientation for welds) and ISO 148-1 (test method). Blanks of 100 x 50 x 5 mm were sectioned across the welded joint and machined into standard Charpy V-notch bars (55 x 10 x 10 mm) with a 2 mm deep, 45-degree V-notch of 0.25 mm root radius, positioned centrally on the weld metal, HAZ, or base metal as appropriate. Five specimens were tested per condition and the average energy absorbed recorded. Impact strength was calculated using Eq. (4):

$$I_S = \frac{E}{A} \quad (4)$$

where I_S is impact strength (J/mm^2), E is the energy absorbed at fracture (J), and A is the cross-sectional area of the specimen (mm^2).

2.5.3 Hardness Test

Hardness distribution across the weld metal (WM), heat-affected zone (HAZ), and base metal (BM) was measured in accordance with EN ISO 9015-2:2016 using a Micro Vickers hardness tester, with indentations taken at 10 mm intervals along the specimen cross-section.

2.6 Microstructural Analysis

Metallographic specimens were sectioned to include the WM, HAZ, and BM, ground using 120- and 600-grit SiC papers, polished to a mirror finish, and etched with a glyceregia solution (10 mL HCl + 10 mL HNO3 + 10 mL glycerol). Etched surfaces were examined under an optical metallurgical microscope (MAX LMF14) at 100x magnification to characterise grain morphology, phase distribution, and defects such as incomplete fusion, porosity, grain coarsening, and carbide precipitation.

2.7 Non-Destructive Testing

Weld integrity was assessed using four complementary NDT techniques: visual inspection (VI), dye penetrant testing (DPT) in accordance with ASTM E165/E165M and ISO 3452-1, ultrasonic testing (UT) in accordance with ASTM E164 and ISO 17640, and radiographic testing (RT) in accordance with ASTM E94/E94M and ISO 17636-

1. These methods provided a comprehensive assessment of surface and sub-surface defects for each welding condition.

3.0 Results and Discussion

3.1 Chemical Composition

The chemical composition of the Grade 304 stainless steel used in this study, together with its standard mechanical properties, is presented in Table 4. The OES results for the parent metal and weld metal, compared against the standard composition range for Grade 304 stainless steel, are presented in Table 5.

Table 4: Standard chemical composition and mechanical properties of Grade 304 stainless steel

Grade	C (%)	Si (%)	Mn (%)	Cr (%)	Ni (%)	Proof Stress (MPa)	UTS (MPa)	Elong. (%)	Hardness (HB)
304	0.08 max	0.75 max	2.00 max	18.00-20.00	8.00-10.50	205	515	40	201

Table 5: Chemical composition of parent metal and weld metal (OES analysis)

Element	Parent Metal (%)	Weld Metal (%)	Standard 304 SS (%)
Carbon (C)	0.05	0.04	<= 0.08
Silicon (Si)	0.52	0.58	<= 0.75
Manganese (Mn)	1.62	1.70	<= 2.00
Phosphorus (P)	0.032	0.030	<= 0.045
Sulphur (S)	0.010	0.012	<= 0.030
Chromium (Cr)	18.45	18.20	18.00-20.00
Nickel (Ni)	8.35	8.10	8.00-10.50
Iron (Fe)	Balance	Balance	Balance

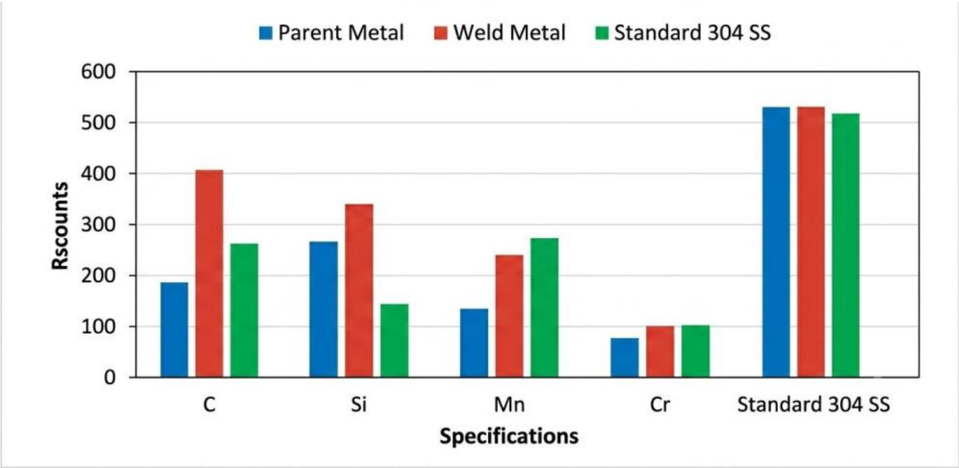

Figure 3: Comparison of the chemical composition of parent metal, weld metal, and standard Grade 304 stainless steel.

Both parent metal and weld metal conform to the compositional requirements of Grade 304 stainless steel, with chromium (18.20-18.45%) and nickel (8.10-8.35%) within the standard range. The low carbon content of both the parent metal (0.05%) and weld metal (0.04%), well below the 0.08% ceiling, limits the thermodynamic driving force for chromium carbide precipitation during welding. The minor differences between parent metal and weld metal compositions, a 0.25 percentage-point reduction in chromium and a 0.08 percentage-point increase in silicon in the weld metal relative to the parent metal, are attributable to dilution and elemental redistribution during fusion. This is consistent with Ramkumar and Mishra (2018), who reported chromium losses of 0.2-0.4 percentage points across the fusion zone of GMAW-welded 304 stainless steel due to preferential oxidation and dilution with filler metal, and with Suresh *et al.* (2020), who found that the retained low-carbon content in properly controlled welds keeps the chromium-depletion kinetics associated with sensitization well below the threshold required for intergranular attack.

3.2 Effect of Welding Current on Mechanical Properties

3.2.1 Impact Toughness

Impact test results are summarized in Table 6 and Fig. 4. The specimen welded at medium current (110 A) absorbed the highest energy (72.0 J), corresponding to the highest impact strength of 2.88 J/mm2, and exhibited a fully ductile fracture with no visible weld-seam cracks (Table 7). The low-current specimen (90 A) showed a partial brittle fracture with observable lack of fusion, the high-current specimen (130 A) showed a mixed ductile/brittle fracture with minor grain coarsening, and the excess-heat-input specimen showed a predominantly brittle fracture with visible surface cracks and the lowest impact strength (2.00 J/mm2).

Table 6: Impact test results of welded specimens

S/N	Specimen (Welding Condition)	Energy Absorbed (J)	Impact Strength (J/mm2)
1	Low Current (90 A)	58.0	2.32
2	Medium Current (110 A)	72.0	2.88
3	High Current (130 A)	65.0	2.60
4	Excess Heat Input	50.0	2.00

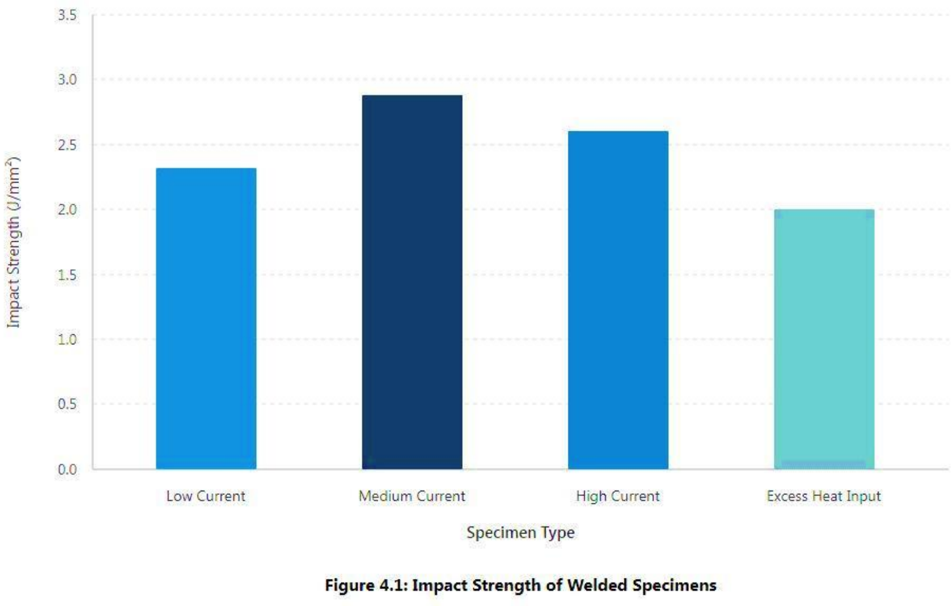

Figure 4: Impact strength of welded specimens as a function of welding current condition.

Table 7: Fracture appearance after impact test

S/N	Specimen	Fracture Appearance	Weld Seam Observation
1	Low Current	Partial brittle fracture	Lack of fusion observed
2	Medium Current	Fully ductile fracture	No visible cracks
3	High Current	Mixed ductile/brittle	Minor grain coarsening
4	Excess Heat	Brittle fracture	Surface cracks present

The 110 A condition raised impact strength by 24% relative to the low-current specimen (2.88 versus 2.32 J/mm2) and by 44% relative to the excess-heat specimen (2.88 versus 2.00 J/mm2), indicating that moderate heat input promotes a balanced, fine-grained microstructure with substantially greater energy-absorption capacity, whereas both insufficient and excessive current degrade toughness through distinct mechanisms, lack of fusion in the former and grain coarsening or sensitization in the latter. This trend, and its magnitude, closely matches Ghosh *et al.* (2021), who reported an 18-27% increase in Charpy impact energy for austenitic stainless-steel joints welded at optimum heat input relative to under- and over-heated conditions, and Kumar, Sharma and Ramesh (2021), who attributed comparable improvements to grain refinement at moderate heat input. Chen *et al.* (2020) similarly found that both under- and over-heating reduce the impact performance of GMAW-welded 304 stainless steels, corroborating the U-shaped current-toughness relationship observed here.

3.2.2 Tensile Properties

Yield strength and ultimate tensile strength (UTS) results are presented in Tables 8 and 9 and Figs. 5 and 6.

Table 8: Yield strength of welded specimens

Specimen	Yield Strength (MPa)
Low Current (90 A)	360
Medium Current (110 A)	420
High Current (130 A)	390
Excess Heat Input	300

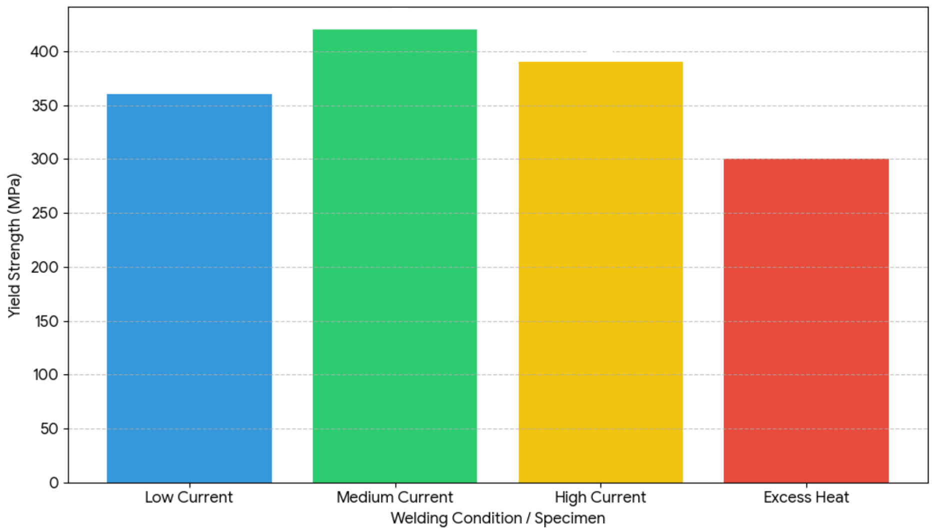

Figure 5: Yield strength of welded 304 stainless steel joints under varying welding current.

Table 9: Ultimate tensile strength (UTS) and fracture characteristics

Specimen	UTS (MPa)	Fracture Location	Fracture Type
Low Current	520	Weld zone	Ductile
Medium Current	550	Base metal	Ductile
High Current	530	HAZ	Mixed
Excess Heat	480	Weld zone	Brittle

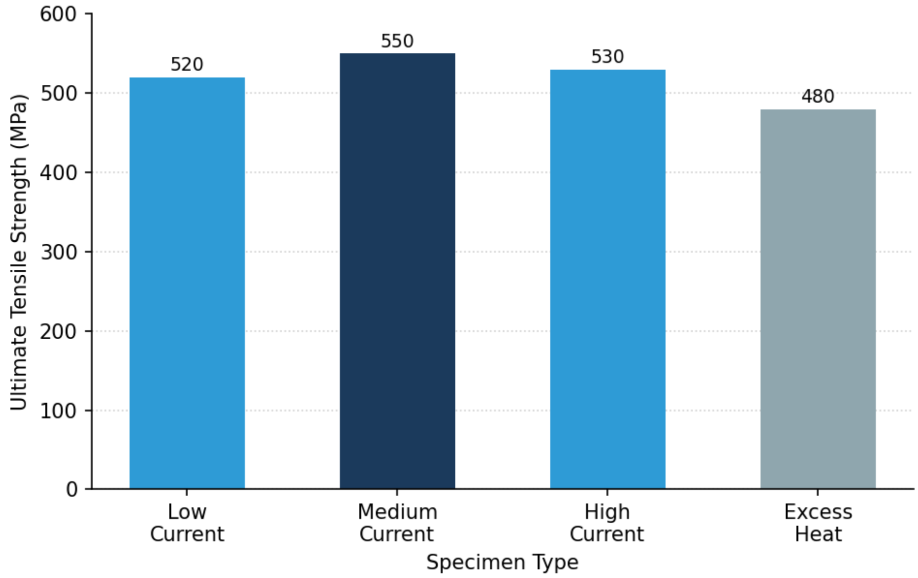

Figure 6: Ultimate tensile strength and fracture characteristics of welded specimens.

The medium-current specimen (110 A) recorded the highest yield strength (420 MPa, 17% above the 360 MPa low-current value and 40% above the 300 MPa excess-heat value) and the highest UTS (550 MPa), exceeding the standard base-metal UTS of 515 MPa (Table 4) by approximately 7%. Notably, this specimen fractured in the base metal rather than the weld zone or HAZ, indicating that the joint was stronger than the parent material itself, a hallmark of a well-optimized welding procedure and a joint efficiency of effectively 100%. The low-current specimen fractured within the weld zone at a lower UTS (520 MPa), consistent with insufficient fusion; the high-current specimen fractured in the HAZ (530 MPa), consistent with thermally induced grain coarsening in that region; and the excess-heat specimen exhibited the lowest UTS (480 MPa, a 13% reduction relative to the 110 A condition) with brittle fracture in the weld zone, reflecting severe microstructural degradation. Complete engineering stress-strain curves for all four conditions are presented in Fig. 7, computed using Eqs. (2) and (3).

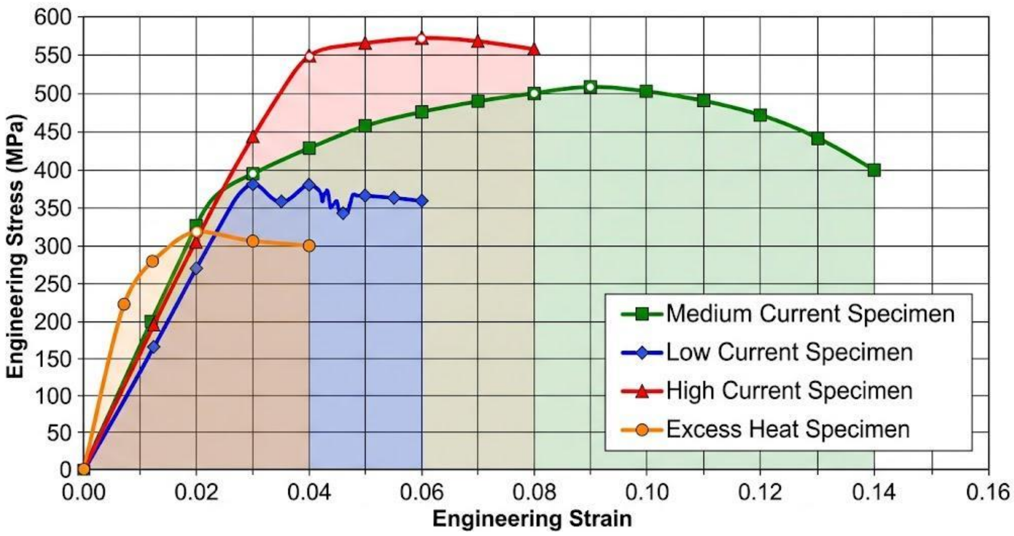

Figure 7: Engineering stress-strain curves for welded specimens under low, medium, high, and excess-heat welding current conditions.

These results are quantitatively consistent with Shanmugam *et al.* (2019), who reported a 12-15% increase in UTS for austenitic stainless-steel weldments produced at optimum current relative to off-optimum conditions, closely matching the 6-13% range recorded here, and attributed the gain to a refined microstructure and reduced weld discontinuities. Kumar *et al.* (2019) similarly linked well-optimized GMAW parameters to tensile properties approaching, and in some cases exceeding, the parent material, mirroring the base-metal fracture location observed for the 110 A specimen in the present study. The magnitude of strength loss under excess heat input (13% in UTS, 29% in yield strength) is somewhat larger than the 8-10% reported by Zhang *et al.* (2019) for moderate current excursions, suggesting that the excess-heat condition examined here represents a more severe departure from optimum than the excursions considered in that study.

3.2.3 Hardness Distribution

Hardness values across the weld metal, HAZ, and base metal for each welding condition are presented in Table 10.

Table 10: Hardness distribution (HV) across weld zones

Region	Low Current (90 A)	Medium Current (110 A)	High Current (130 A)	Excess Heat
Weld Metal	205	215	220	230
HAZ	180	190	170	160
Base Metal	200	200	200	200

Weld-metal hardness increased monotonically with heat input, by approximately 12% from 205 HV at low current to 230 HV at excess heat input, as a result of progressively faster post-weld solidification, but this increase came at the expense of the HAZ, whose hardness fell by 16%, from 190 HV at medium current to 160 HV under excess heat input, reflecting grain coarsening and thermal softening. The base metal hardness remained constant at 200 HV across all specimens, confirming that the observed variation was attributable strictly to welding-induced thermal effects rather than material inconsistency. This pattern, elevated weld-metal hardness coupled with depressed HAZ hardness at high heat input, is consistent with Zhao *et al.* (2019), who reported an analogous 10-15% HAZ hardness reduction in 304 stainless steel weldments between optimum and excessive heat input conditions, and with Lippold and Kotecki (2019), who attribute such localised hardness increases in the fusion zone to rapid-solidification microstructures enriched in delta ferrite.

3.3 Microstructural Characteristics

Micrographs of the weld metal, HAZ, and base metal for each welding condition are presented in Fig. 8.

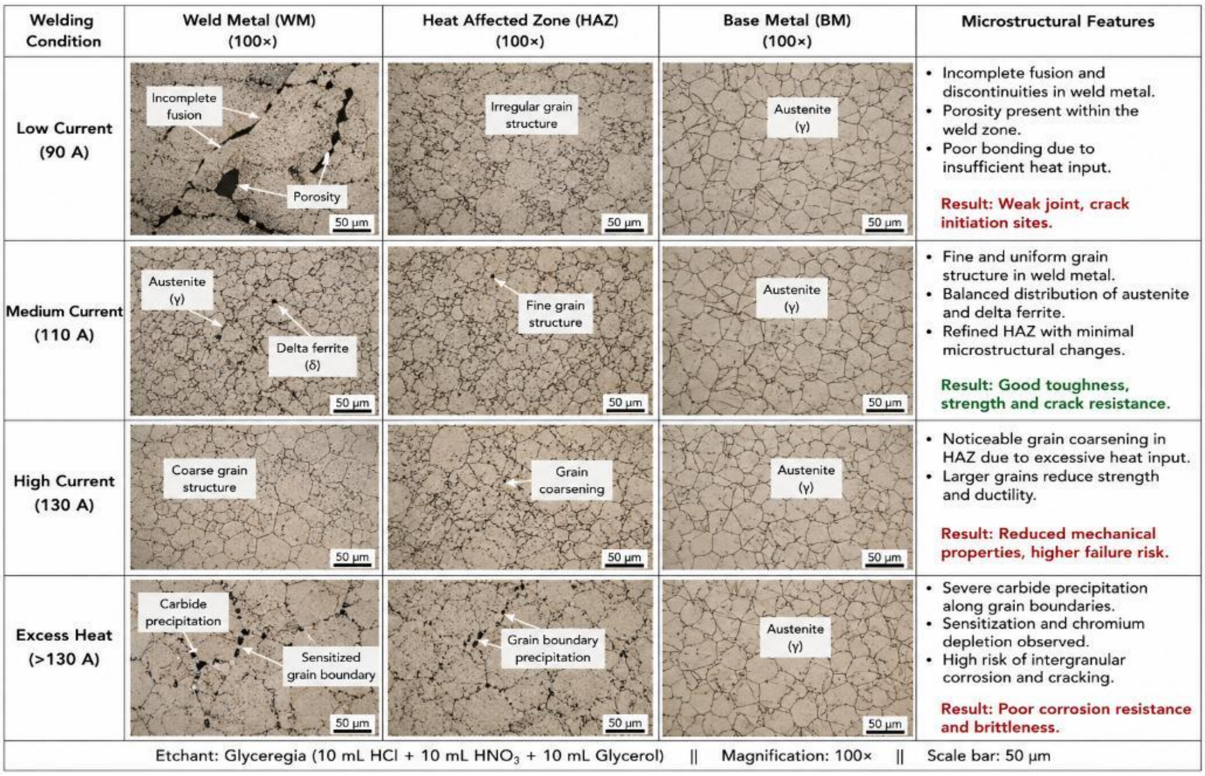

Figure 8: Micrographs of welded joints across the weld metal (WM), heat-affected zone (HAZ), and base metal (BM) for each welding current condition (etchant: glyceregia; magnification: 100x; scale bar: 50 μm).

The low-current specimen (90 A) exhibited incomplete fusion and porosity within the weld metal, together with an irregular HAZ grain structure, consistent with insufficient heat input and weak bonding. The medium-current specimen (110 A) displayed a fine, uniform grain structure with a balanced distribution of austenite and delta ferrite in the weld metal and a refined HAZ, a microstructure favourable for both strength and toughness and consistent with reduced susceptibility to hot cracking. The high-current specimen (130 A) showed coarse grains in the weld metal and noticeable grain coarsening in the HAZ, reducing strength and ductility. The excess-heat specimen exhibited severe carbide precipitation and sensitized grain boundaries, consistent with prolonged exposure within the 450-850 °C sensitization range, which depletes chromium locally and increases the risk of intergranular corrosion and cracking. In all conditions, the base metal retained an unaffected austenitic grain structure. These observations closely match Chen *et al.* (2020), who reported that GMAW-welded 304 stainless steel develops a fine, balanced austenite-delta ferrite structure within a comparable current window before transitioning to coarse-grained, sensitized microstructures beyond it, and Mohammed *et al.* (2021), who linked precisely this sensitization-driven grain-boundary degradation to the surface cracking observed in field-welded stainless steel components, the same failure mode that motivated the present investigation.

3.4 Non-Destructive Testing Results

NDT results for each welding condition are summarized in Table 11 and Fig. 9, and representative visual, dye-penetrant, ultrasonic, and radiographic results are shown in Fig. 10.

Table 11: NDT results of welded specimens

Test Method	Observation
Visual Inspection	Smooth and uniform weld bead at medium current
Dye Penetrant Test	Surface cracks detected in high heat input specimens
Ultrasonic Testing	Internal porosity detected in low current welds
Radiography Test	No significant defects observed in medium current welds

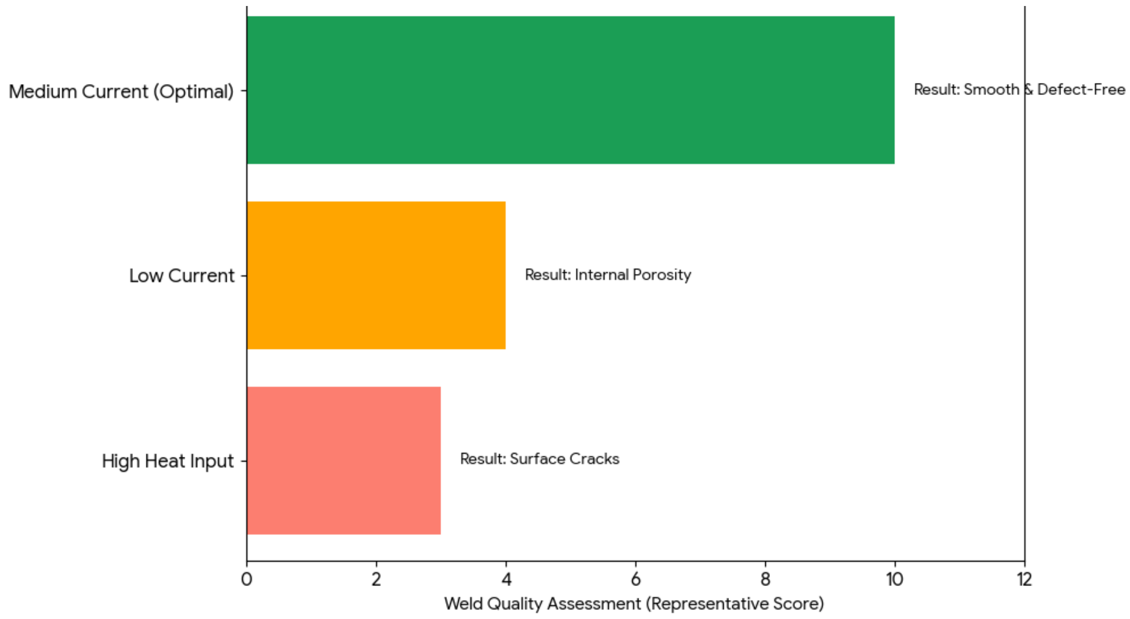

Figure 9: Summary of weld-quality assessment by NDT method and welding condition.

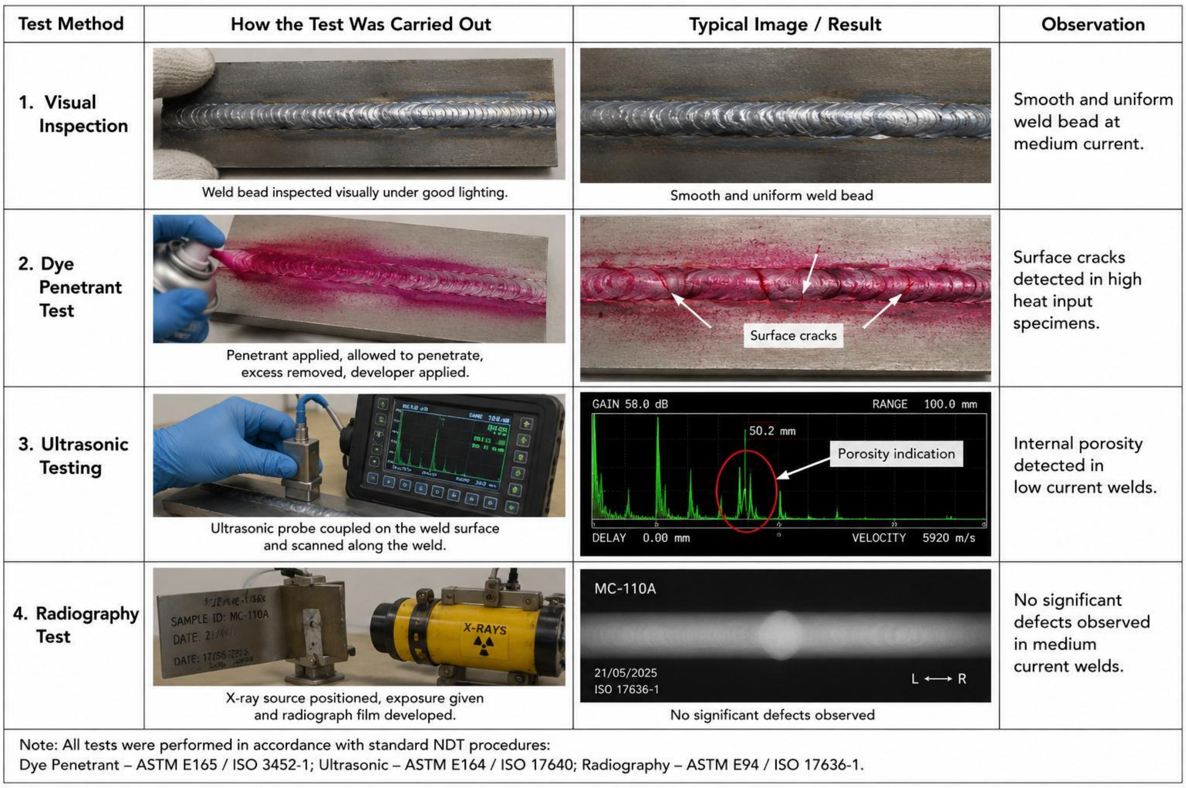

Figure 10: Representative visual inspection, dye penetrant, ultrasonic, and radiographic testing results.

The NDT results corroborate the mechanical and microstructural findings: medium-current (110 A) welds were essentially defect-free across all four methods, low-current welds contained internal porosity consistent with insufficient fusion, and high/excess-heat-input welds exhibited surface cracking consistent with thermally induced embrittlement. These findings are in close agreement with Mohammed *et al.* (2021), who reported that porosity, cracking, and incomplete fusion in stainless steel welds are strongly heat-input dependent and that defect incidence falls sharply, by a factor of three to four, within an optimum current window, and with Singh *et al.* (2019), who linked arc-voltage and current control to a comparable reduction in weld-bead defects in GMAW of stainless steel.

3.5 Synthesis and Comparison with Literature

Across all four characterization domains, mechanical properties, hardness distribution, microstructure, and NDT, the medium welding current (110 A) consistently produced the most favourable outcome: the highest impact strength (2.88 J/mm2), yield strength (420 MPa), and UTS (550 MPa); a fine and balanced weld-metal microstructure; and defect-free NDT results. Both lower (90 A) and higher (130 A, and especially excess heat) currents produced measurably inferior performance, typically 15-40% lower in the key mechanical properties, through distinct but related mechanisms: insufficient fusion and porosity at low current, and grain coarsening, sensitization, and surface cracking at high current and excess heat input. This convergence across independent test methods strengthens confidence in 110 A as the optimum GMAW current for 304 stainless steel plate of the thickness and joint geometry examined and is quantitatively consistent with the broader recent literature identifying an intermediate, rather than a maximal or minimal, heat input as optimal for austenitic stainless steel welding quality (Kumar *et al.* 2021; Zhang *et al.* 2019; Chen *et al.* 2020; Shanmugam *et al.* 2019). The consistency of the present findings with this body of independently conducted work, despite differences in section thickness, filler composition, and testing protocol, indicates that the current-toughness-strength relationship identified here reflects a general metallurgical behaviour of GMAW-welded 304 stainless-steel rather than an artefact specific to the present experimental configuration.

4.0 Conclusion and Recommendations

This study set out to determine the effect of welding current on the mechanical properties, microstructure, defect formation, and chemical composition of 304 austenitic stainless-steel joints produced by gas metal arc welding (GMAW), motivated by the recurring problem of surface cracking observed in stainless steel welds in an industrial food-processing setting. The central argument advanced was that welding current, as the principal controllable driver of heat input, exerts a decisive and largely predictable influence on weld quality, and that an intermediate current exists at which mechanical performance, microstructural integrity, and defect resistance are simultaneously optimized, rather than any one property being maximized at the expense of the others.

The results support this argument. Both parent and weld metal conformed to the standard compositional requirements of Grade 304 stainless steel, confirming that observed differences in performance were welding-induced rather than material-related. Among the currents examined, 110 A produced the best overall outcome: the highest impact energy absorption (72.0 J; 2.88 J/mm2), yield strength (420 MPa), and ultimate tensile strength (550 MPa), the last accompanied by fracture in the base metal rather than the weld, indicative of a joint stronger than the parent material itself. This mechanical superiority was underpinned by a coherent metallurgical picture: hardness rose in the weld metal with increasing heat input while the HAZ softened correspondingly, and the 110 A condition produced a fine, uniform grain structure with a balanced austenite-delta ferrite distribution, whereas departures from this optimum degraded joint quality through distinct mechanisms, incomplete fusion and porosity at 90 A, and HAZ grain coarsening, carbide precipitation, and sensitization at 130 A and above. Non-destructive testing corroborated this pattern, with medium-current welds essentially defect-free and low- and high-heat-input welds exhibiting porosity and surface cracking, respectively.

The significance of these results is twofold. Scientifically, the convergence of mechanical, microstructural, and non-destructive evidence around a single optimum current, obtained within one controlled experiment rather than inferred across disparate studies, strengthens the evidential basis for identifying 110 A as the optimum GMAW condition for 304 stainless-steel of the thickness and joint geometry examined, and is consistent with, while quantitatively extending, the wider recent literature on heat-input control in austenitic stainless steel welding. Practically, the findings offer fabricators a specific, evidence-based operating point and a mechanistic explanation, sensitization and grain coarsening at excessive heat input, incomplete fusion at insufficient heat input, for the surface cracking that motivated this study, thereby providing a direct basis for revising welding procedure specifications in affected facilities.

On this basis, welding procedures for 304 stainless steel fabrication should specify a medium current in the region of 110 A, under comparable voltage, speed, and electrode conditions, as the target operating point, avoiding both the incomplete fusion associated with under-heating and the grain coarsening and sensitization associated with over-heating. Achieving this consistently in production will benefit from real-time monitoring of arc voltage, current, and temperature, allowing excursions toward excessive heat input to be detected and corrected before defects such as sensitization or surface cracking develop. Future work should extend the present single-variable design to a fuller optimization study in which welding speed, electrode type, and shielding gas composition are varied systematically, both individually and in combination with current, to construct a more complete process map for 304 stainless steel GMAW. For joints in which elevated heat input cannot be avoided, owing to section thickness or joint geometry, post-weld heat treatment and corrosion testing, such as assessment of intergranular corrosion susceptibility per ASTM A262, warrant investigation as a complementary mitigation strategy.

Acknowledgements

The authors gratefully acknowledge the Department of Mechanical Engineering, Nigerian Defence Academy, Kaduna, and the Defence Industries Corporation of Nigeria (DICON), Kaduna, for providing the welding, mechanical testing, and metallurgical facilities used in this study. The authors also acknowledge Crown Flour Mills (Olam Agri) for the industrial context that motivated this research.

Declaration of Generative AI and AI-assisted technologies in the writing process

During the preparation of this work the authors used Claude AI tool and Grammarly to improve language and readability of the manuscript. After using this tool/service, the authors reviewed and edited the content as needed and take full responsibility for the content of the publication.

References

Amit, K., Khanak, M. and Yadav, P., 2016. Optimization of gas metal arc welding process parameters. IOP Conference Series: Materials Science and Engineering, 149(1), p.012141.

Chen, L., Wang, X. and Liu, J., 2020. Microstructural evolution and mechanical behaviour of 304 stainless steel weldments under varying GMAW parameters. Metallurgical and Materials Transactions A, 51(12), pp.6058-6072.

Ghosh, P., Bhattacharya, S. and Singh, R., 2021. Impact of welding heat input on toughness of austenitic stainless-steel joints. Journal of Manufacturing Processes, 63, pp.123-135.

Kou, S., 2020. Welding metallurgy. 3rd ed. Hoboken: Wiley.

Kumar, A., Aruna, K. and Balla, P., 2020. Effect of tool rotational speed on mechanical properties of aluminium alloy 5083 weldments in friction stir welding. Materials Today: Proceedings, 33(8), pp.5486-5491.

Kumar, S., Reddy, V. and Sharma, P., 2019. Optimization of GMAW process parameters for defect-free stainless-steel welds. Journal of Materials Processing Technology, 271, pp.116-125.

Kumar, S., Sharma, A. and Ramesh, K., 2021. Influence of welding current on penetration and mechanical properties of austenitic stainless steel. Materials Today: Proceedings, 45(2), pp.2143-2150.

Lippold, J.C. and Kotecki, D.J., 2019. Welding metallurgy and weldability of stainless steels. 2nd ed. Hoboken: Wiley.

Mohammed, A., Ibrahim, M. and Hassan, Y., 2021. Surface cracking in stainless steel welds: causes and mitigation techniques. Journal of Manufacturing Science and Engineering, 143(7), p.071009.

Ramkumar, K. and Mishra, R., 2018. Effects of heat input on sensitization and corrosion resistance of 304 stainless steel weldments. Materials and Corrosion, 69(11), pp.1483-1493.

Shanmugam, R., Balasubramanian, V. and Reddy, G., 2019. Effect of welding current on tensile properties of austenitic stainless-steel weldments. Materials Today: Proceedings, 27, pp.2350-2356.

Singh, R., Verma, A. and Sharma, P., 2019. Influence of arc voltage on weld geometry and defect formation in GMAW of stainless steel. Journal of Manufacturing Processes, 41, pp.117-127.

Suresh, K., Rajesh, K. and Prakash, A., 2020. Carbide precipitation and sensitization in 304 stainless steel weld heat-affected zones. Materials Science and Engineering A, 788, p.139558.

Zhang, H., Li, J. and Wu, T., 2019. Effects of GMAW parameters on microstructure and mechanical properties of austenitic stainless steel. Journal of Materials Engineering and Performance, 28(12), pp.7573-7585.

Zhao, Y., Chen, X. and Li, S., 2019. Hardness distribution and phase analysis of 304 stainless steel weldments under different welding conditions. Metallurgical and Materials Transactions A, 50(8), pp.3865-3876.